Stererographic imaging condition for wave-equation migration

Paul Sava, Center for Wave Phenomena, Colorado School of Mines

SUMMARY

Single-scattering imaging consists of two steps: wavefield extrapolation, to reconstruct source and receiver wavefields from recorded data, and imaging, to extract from the extrapolated wavefields the locations where reflectors occur. Conventionally, the imaging condition indicates the presence of reflectors when the propagation time of reflections in the source and receiver wavefields match. The main drawback of conventional cross-correlation imaging condition is that it ignores the local spatial coherence of reflection events and relies on their propagation time. This leads to interference (cross-talk) between unrelated events that occur at the same time. Sources of cross-talk include seismic events corresponding to different seismic experiments, seismic events corresponding to different propagation paths, etc. An alternative imaging condition operates on the same extrapolated wavefields, but cross-correlation takes place in a higher-dimensional domain where seismic events are separated based on their local space-time slope. Events are matched based on two parameters (time and local slope), thus justifying the name "stereographic" for this imaging condition. Stereographic imaging attenuates cross-talk and reduces imaging artifacts compared with conventional imaging.

INTRODUCTION

Conventional depth migration consists of two steps: wavefield extrapolation used to reconstruct the seismic wavefields at all locations in the imaging volume from data recorded on the acquisition surface, and imaging used to extract reflectivity information from wavefields extrapolated from the sources and receivers.

Accurate imaging requires accurate implementation of both steps. Recent seismic imaging research places larger emphasis on wavefield extrapolation than on imaging. This paper concentrates on the imaging condition assuming that wavefield extrapolation can be performed with sufficient accuracy. The imaging condition is often implemented as a cross-correlation or deconvolution of source and receiver wavefields extrapolated from the acquisition surface (Claerbout, 1985). The reason for this choice is that conventional cross-correlation imaging is fast and robust, producing good images in complex environments.

Conventional imaging condition operates in a simple way: source and receiver wavefields are probed to determine the locations where they match, i.e. where the traveltime of events simulated from the source and back-propagated from the receivers are equal. This is usually achieved by extracting the zero-lag of the temporal cross-correlation between the two wavefields computed at every location in the image. This imaging condition ignores the structure of the analyzed seismic wavefields, i.e. the imaging condition does not use the local space-time coherence of the reflected wavefields. This is a striking feature, since analysis of space-time kinematic coherence is one of the most important attributes employed in analysis of seismic data.

The consequence of this is that different seismic events present in the extrapolated wavefields interfere with one-another leading to artifacts in seismic images. This interference, also know as cross-talk, can occur between unrelated events. It is often possible to identify events that occur at the same time, although they describe different propagation paths in the subsurface. As a consequence, such unrelated events appear as real reflections due to the imaging condition.

This paper presents an extension of the conventional imaging condition designed to exploit the local space-time coherence of extrapolated wavefields. Different seismic events are matched not only function of propagation time, but also function of their local coherence attributes, e.g. local slope measured function of position and time. The consequence is that events with different propagation paths are distinguished from one-another, although their propagating time to a given point in the subsurface may be identical.

CONVENTIONAL IMAGING CONDITION

Under the single scattering (Born) assumption, seismic imaging consists of two components: The first component is *wavefield extrapolation* which represents a solution to the considered (acoustic) wave-equation with recorded data as boundary condition. We can consider many different numeric solutions to the acoustic wave-equation, which are distinguished, for example, by implementation domain (space-time, frequency-wavenumber, etc.) or type of numeric solution (differential, integral, etc.). Irrespective of numeric implementation, we reconstruct using wavefield extrapolation two wavefields, one extrapolated from the source and one extrapolated from the receiver locations. Those wavefields can be represented as four-dimensional objects function of position in space $\mathbf{x} = (x, y, z)$ and time t

$$U_S = U_S(\mathbf{x}, t) \tag{1}$$
$$U_R = U_R(\mathbf{x}, t) \ , \tag{2}$$

where U_S and U_R denote source and receiver wavefields.

The second imaging component is the *imaging condition* which is designed to extract from the extrapolated wavefields (U_S and U_R) the locations where reflectors occur in the subsurface. A conventional imaging condition Claerbout (1985) exploits the similarities between the source and receiver wavefields. Thus, an image is formed when the zero-lag of the temporal cross-correlation between U_S and U_R maximizes. This imaging condition can be represented mathematically as

$$R(\mathbf{x}) = \int U_S(\mathbf{x}, t)\, U_R(\mathbf{x}, t)\, dt \ , \tag{3}$$

where R represents the image function of position $\mathbf{x}$.

This conventional imaging condition uses the match between source and receiver wavefields U_S and U_R along the time axis, independently at every location in space. Thus, the conventional imaging condition represents a special case of an extended imaging condition which uses the similarities between the source and receiver wavefields on all 4 dimensions, space $\mathbf{x}$ and time t. More generally, the source and receiver wavefields are coincident (form an image) if the local cross-correlation between the source and receiver wavefields maximizes at zero-lag on all four dimensions. An extended imaging condition (Sava and Fomel, 2005, 2006) can be formulated mathematically as

$$R(\mathbf{x}, 2\mathbf{l}, 2\tau) = \int U_S(\mathbf{x} - \mathbf{l}, t - \tau)\, U_R(\mathbf{x} + \mathbf{l}, t + \tau)\, dt \ , \tag{4}$$

where $\mathbf{l}$ and τ represent the spatial and temporal cross-correlation lags between the source and receiver wavefields. Other extended imaging conditions (Rickett and Sava, 2002; Biondi and Symes, 2004) represent special cases of the extended imaging condition corresponding to horizontal $\mathbf{l} = (l_x, l_y, 0)$, or vertical $\mathbf{l} = (0, 0, l_z)$ space lags, respectively.

The four-dimensional cross-correlation maximizes at zero lag if the wavefields are correctly reconstructed. If the source and receiver wavefields are inaccurately reconstructed, either because we are using an

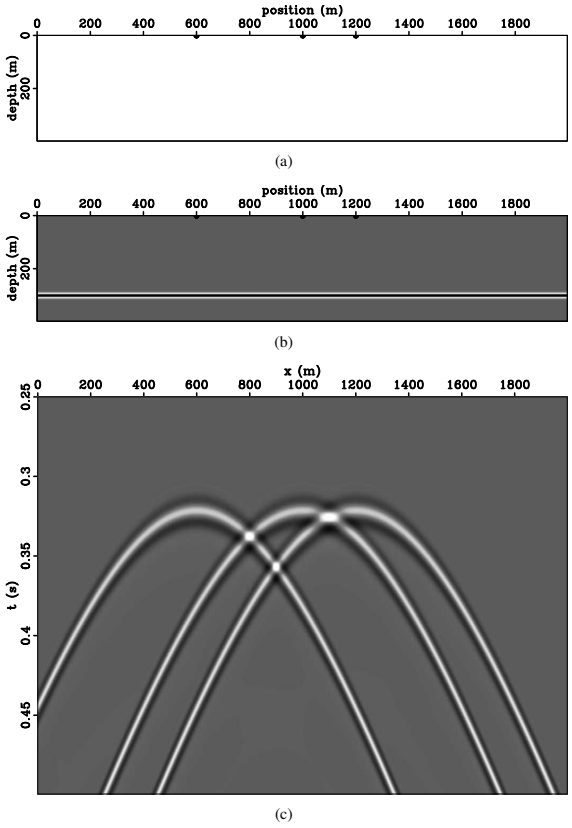

Figure 1: Constant velocity model (a), reflectivity model (b), data (c) and shot locations at $x = 600, 1000, 1200$ m).

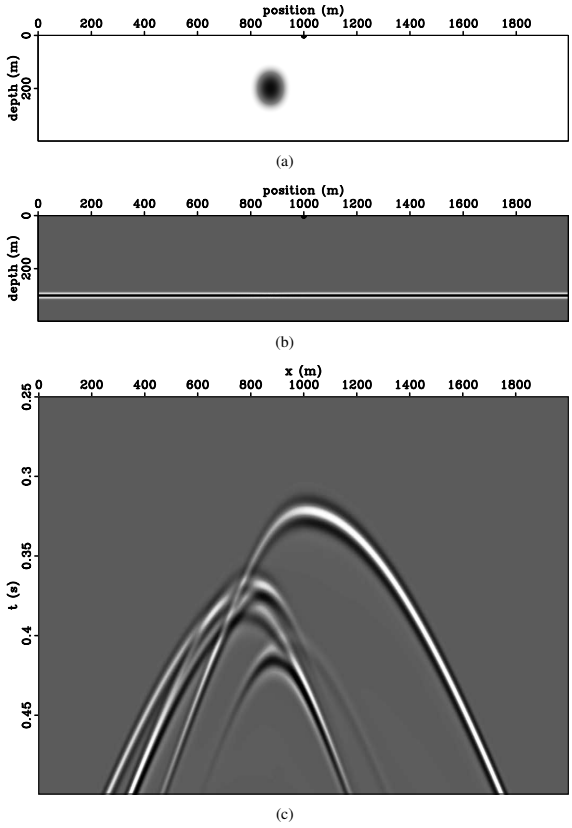

Figure 2: Velocity model with a negative Gaussian anomaly (a), reflectivity model (b), data (c) and shot location at $x = 1000$ m).

approximate extrapolation operator (e.g. one-way extrapolator with limited angular accuracy), or because the velocity used for extrapolation is inaccurate, the four-dimensional cross-correlation does not maximize at zero lag. In this case, part of the cross-correlation energy is smeared over the space and time lags ($\mathbf{l}$ and τ), therefore extended imaging conditions can be used to evaluate imaging accuracy, for example by decomposition of reflectivity function of scattering angle at every image location (Sava and Fomel, 2003; Biondi and Symes, 2004; Sava and Fomel, 2006). Angle-domain images carry information useful for migration velocity analysis (Biondi and Sava, 1999; Sava and Biondi, 2004a,b; Shen et al., 2005), or for amplitude analysis (Sava et al., 2001), or for attenuation of multiples (Sava and Guitton, 2005; Artman et al., 2007)

The conventional imaging condition (3) is the focus of this paper. As discussed above, assuming accurate extrapolation, this imaging condition should produce accurate images at zero cross-correlation lags. However, this conclusion does not always hold true, as illustrated next.

Figures 1(a) and 1(b) represent a simple model of constant velocity with a horizontal reflector. Data in this model are simulated from 3 sources triggered simultaneously at coordinates $x = 600, 1000, 1200$ m. Using the standard imaging procedure outlined in the preceding paragraphs, we can reconstruct the source and receiver wavefields, U_S and U_R, and apply the conventional imaging condition equation (3) to obtain the image in figure 3(a). The image shows the horizontal reflector superposed with linear artifacts of comparable strength.

Figures 2(a) and 2(b) represent another simple model of spatially variable velocity with a horizontal reflector. Data in this model are simulated from a source located at coordinate $x = 1000$ m. The negative Gaussian velocity anomaly present in the velocity model creates triplications of the source and receiver wavefields. Using the same standard imaging procedure outlined in the preceding paragraphs, we obtain the image in figure 4(a). The image shows the horizontal reflector superposed with complex artifacts of comparable strength.

In both cases discussed above, the velocity model is perfectly known and the acoustic wave equation is solved with the same finite-difference operator implemented in the space-time domain. Therefore, the artifacts are caused only by properties of the conventional imaging condition used to produce the migrated image and not by inaccuracies of wavefield extrapolation or of the velocity model.

The cause of artifacts is *cross-talk* between unrelated events present in the source and receiver wavefields, which are not supposed to match, For example, cross-talk can occur between wavefields corresponding to multiple sources, as illustrated in the example shown in figures 1(a)-1(b), multiple branches of a wavefield corresponding to one source, as illustrate in the example shown in figures 2(a)-2(b), events that correspond to multiple reflections in the subsurface, or multiple wave modes of an elastic wavefield, for example between PP and PS reflections, etc.

STEREOGRAPHIC IMAGING CONDITION

One possibility to remove the artifacts caused by the cross-talk between unrelated events in the wavefield is to modify the imaging condition to use more than one attribute to match events in the source and receiver wavefields. For example, we could use the time and slope to match events in the wavefield, thus distinguishing between unrelated events that occur at the same time.

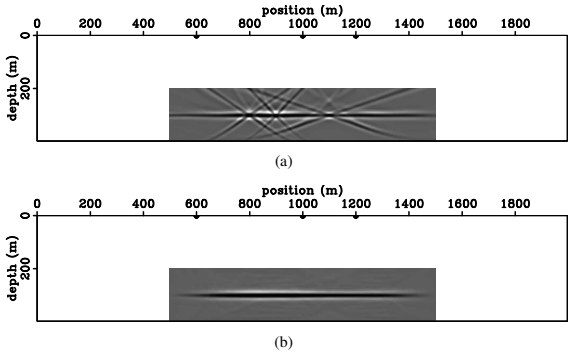

Figure 3: Images obtained for the model in figures 1(a)-1(c) using the conventional imaging condition (a) and the stereographic imaging condition (b).

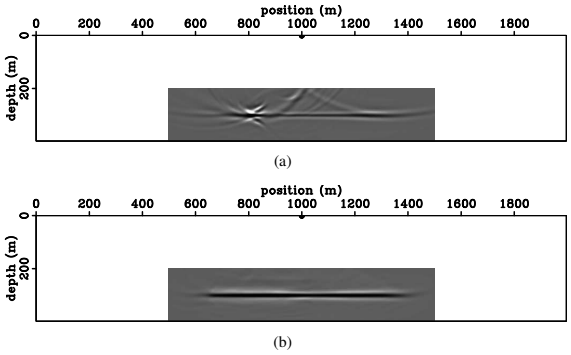

Figure 4: Images obtained for the model in figures 2(a)-2(c) using the conventional imaging condition (a) and the stereographic imaging condition (b).

One way of decomposing the source and receiver wavefields function of local slope at every position and time is by local slant-stacks at coordinates $\mathbf{x}$ and t in the four-dimensional source and receiver wavefields. Thus, we can write the total source and receiver wavefields (U_S and U_R) as a sum of the decomposed wavefields (W_S and W_R):

$$U_S(\mathbf{x},t) = \int W_S(\mathbf{x},\mathbf{p},t)\,d\mathbf{p} \quad (5)$$

$$U_R(\mathbf{x},t) = \int W_R(\mathbf{x},\mathbf{p},t)\,d\mathbf{p}\,. \quad (6)$$

Here $\mathbf{p}$ represents the local slope function of position and time. Using the wavefields decomposed function of local slope, W_S and W_R, we can design a stereographic imaging condition which is mathematically represented by an expression like

$$R(\mathbf{x}) = \int\int W_S(\mathbf{x},\mathbf{p},t)\,W_R(\mathbf{x},\mathbf{p},t)\,d\mathbf{p}dt\,. \quad (7)$$

The choice of the word "stereographic" for this imaging condition is analogous to the similar choice made for the velocity estimation method called stereotomography (Billette and Lambare, 1997; Billette et al., 2003) which also employs two parameters (time and slope) to constrain traveltime seismic tomography.

For comparison with the stereographic imaging condition (7), we can reformulate the conventional imaging condition using the wavefield notation (5)-(6) as follows:

$$R(\mathbf{x}) = \int \left[\int W_S(\mathbf{x},\mathbf{p},t)\,d\mathbf{p}\right]\left[\int W_R(\mathbf{x},\mathbf{p},t)\,d\mathbf{p}\right] dt\,. \quad (8)$$

The main difference between imaging conditions (7) and (8) is that in one case we are comparing independent slope components of the wavefields separated from one-another, while in the other case we are comparing a superposition of them, thus not being able to distinguish between waves propagating in different directions. This situation is analogous to that of reflectivity analysis function of scattering angle at image locations, in contrast with reflectivity analysis function of acquisition offset at the surface. In the first case, waves propagating in different directions are separated from one-another, while in the second case all waves are superposed in the data, thus leading to imaging artifacts (Stolk and Symes, 2004).

Figure 3(b) shows the image produced by stereographic imaging of the data generated for the model depicted in figures 1(a)-1(b), and figure 4(b) shows the similar for the model depicted in figures 2(a)-2(b). Images 3(b) and 4(b) use the same source receiver wavefields as images 3(a) and 4(a), respectively. In both cases, the cross-talk artifacts have been eliminated by the stereographic imaging condition.

EXAMPLE

The stereographic imaging condition is illustrated with an example derived from the Sigsbee 2A dataset (Paffenholz et al., 2002). Using the model in figure 5(g), two shots are simulated by wavefield extrapolation modeling, figures 5(a)-5(c), and a third shot is synthesized by summing the two shots together, figure 5(e). Migration with conventional imaging condition of the three shots produces the images in figures 5(b)-5(f). The two shots independently illuminate different parts of the model, figures 5(b)-5(d), while the third composite shot illuminates both sides of the image, figure 5(f). The image produced by the composite shot is populated with artifacts due to the cross-talk between the wavefields originating at the two shot locations.

Figure 5(h) shows the image obtained by imaging the composite shot, figure 5(e), using the stereographic imaging condition. The image is free of artifacts and shows reflectors extending over the entire image, as would be expected for illumination from two shots at different locations. In this case, the stereographic imaging condition needs to take into account the local dip of the image. Since we cannot know the reflector dip prior to the application of the imaging condition, we need to loop over a range of possible dip angles and decompose the wavefields locally for all possible slope combinations.

CONCLUSIONS

Conventional imaging condition based on cross-correlation of extrapolated wavefields does not take into account the local spatial coherence of reflection events. Events are matched based on their propagation times, which leads to cross-talk between unrelated events. The stereographic imaging condition introduced in this paper operates on seismic wavefields that are first decomposed function of their local slope in space and time. Events are matched based on two parameters (time and local slope), which separates unrelated events and eliminates cross-talk. Higher imaging accuracy is achieved at the expense of larger computational cost. Applications include simultaneous imaging of different seismic experiments (shots), multiple attenuation, etc.

ACKNOWLEDGMENT

I acknowledge the support of the sponsors of the Center for Wave Phenomena at Colorado School of Mines.

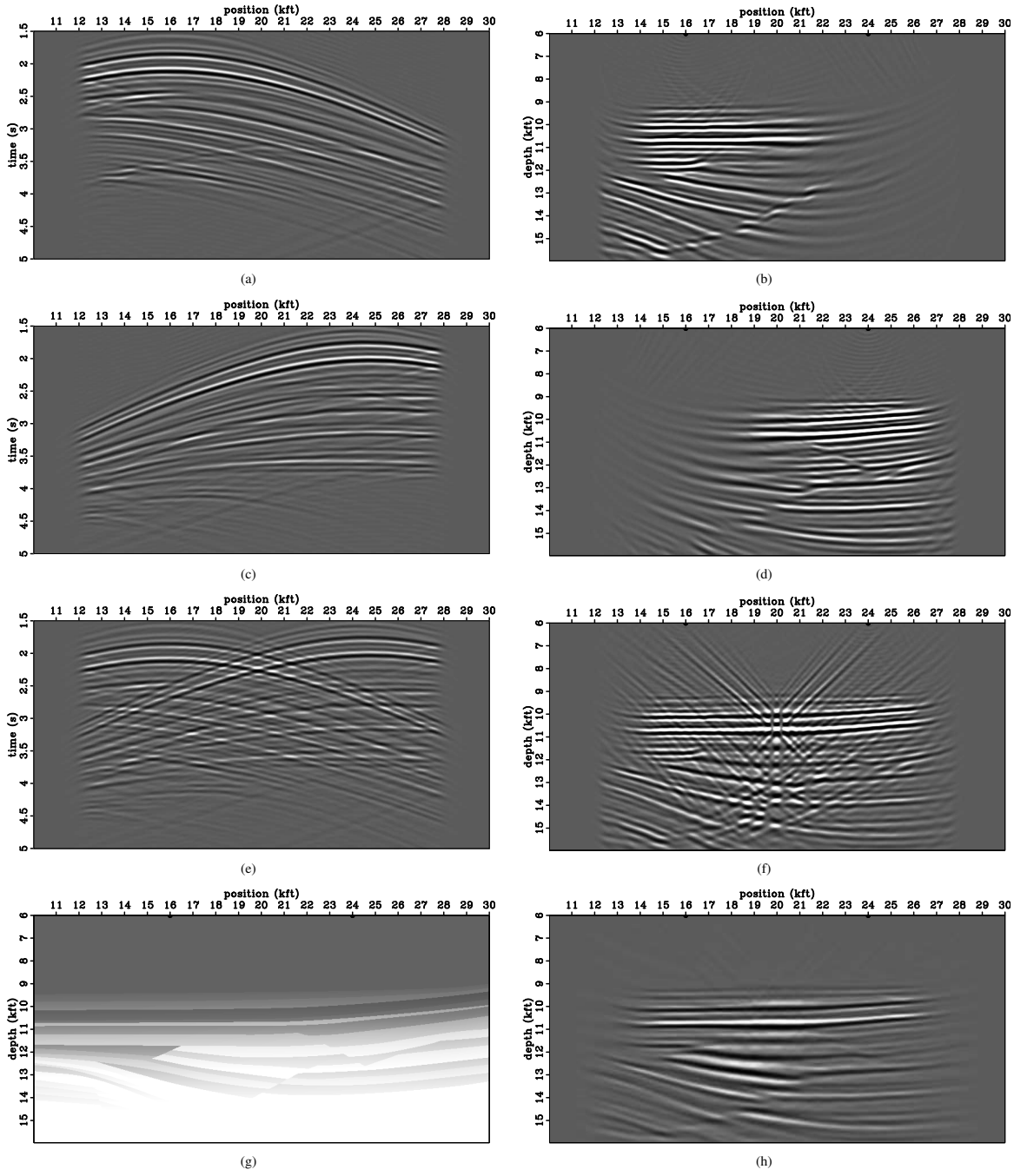

Figure 5: Data corresponding to shots at locations $x = 16$ kft (a), $x = 24$ kft (c), and the sum of data for both shots (d). Image obtained by conventional imaging condition for the shots at locations $x = 16$ kft (b), $x = 24$ kft (d) and the sum of data for both shots (e). $v(z)$ model extracted from the Sigsbee 2A model and shot locations at $x = 16, 24$ kft (f) and image from the sum of the shots located at $x = 16$ kft and $x = 24$ kft obtained using the stereographic imaging condition (g).

REFERENCES

Artman, B., G. Alvarez, and K. Matson, 2007, Image-space surface-related multiple prediction: Geophysics, **72**, S113–S122.

Billette, F., S. L. Begat, P. Podvin, and G. Lambare, 2003, Practical aspects and applications of 2D sterotomography: Geophysics, **68**, 1008–1021.

Billette, F. and G. Lambare, 1997, Velocity macro model estimation by stereotomography: 59th Mtg., Session:P095.P095, Eur. Assn. Geosci. Eng.

Biondi, B. and P. Sava, 1999, Wave-equation migration velocity analysis: 69th Ann. Internat. Meeting, Expanded Abstracts, 1723–1726, Soc. of Expl. Geophys.

Biondi, B. and W. W. Symes, 2004, Angle-domain common-image gathers for migration velocity analysis by wavefield-continuation imaging: Geophysics, **69**, 1283–1298.

Claerbout, J. F., 1985, Imaging the Earth's interior: Blackwell Scientific Publications.

Paffenholz, J., B. McLain, J. Zaske, and P. Keliher, 2002, Subsalt multiple attenuation and imaging: Observations from the Sigsbee2B synthetic dataset: 72nd Ann. Internat. Mtg, 2122–2125, Soc. of Expl. Geophys.

Rickett, J. and P. Sava, 2002, Offset and angle-domain common image-point gathers for shot-profile migration: Geophysics, **67**, 883–889.

Sava, P. and B. Biondi, 2004a, Wave-equation migration velocity analysis - I: Theory: Geophysical Prospecting, **52**, 593–606.

———, 2004b, Wave-equation migration velocity analysis - II: Subsalt imaging examples: Geophysical Prospecting, **52**, 607–623.

Sava, P., B. Biondi, and S. Fomel, 2001, Amplitude-preserved common image gathers by wave-equation migration: 71st Ann. Internat. Mtg., Expanded Abstracts, 296–299, Soc. of Expl. Geophys.

Sava, P. and S. Fomel, 2003, Angle-domain common image gathers by wavefield continuation methods: Geophysics, **68**, 1065–1074.

———, 2005, Coordinate-independent angle-gathers for wave equation migration: 75th Ann. Internat. Mtg., Expanded Abstracts, 2052–2055, Soc. of Expl. Geophys.

———, 2006, Time-shift imaging condition in seismic migration: Geophysics, **71**, S209–S217.

Sava, P. and A. Guitton, 2005, Multiple attenuation in the image space: Geophysics, **70**, V10–V20.

Shen, P., W. W. Symes, S. Morton, and H. Calandra, 2005, Differential semblance velocity analysis via shot profile migration: 2249–2253.

Stolk, C. C. and W. W. Symes, 2004, Kinematic artifacts in prestack depth migration: Geophysics, **69**, 562–575.